IMPACT CRATERING ON CERES: THE SIMPLE–TO–COMPLEX TRANSITION. T. Platz[1,2], A. Nathues[1], M. Schäfer[1], P. Schenk[3], T. Kneissl[4], M. Hoffmann[1], N. Schmedemann[4], H. Hiesinger[5], M.V. Sykes[2], C. A. Raymond[6], C.T. Russell[7]. [1]Max Planck Institute for Solar System Research, Justus-von-Liebig-Weg 3, 37077 Göttingen, Germany (platz@mps.mpg.de); [2]Planetary Science Institute, Tucson, USA; [3]Lunar & Planetary Institute, Houston, USA; [4]Freie Universität Berlin, Berlin, Germany; [5]University of Münster, Münster, Germany; [6]Jet Propulsion Laboratory, Pasadena, USA; [7]University of California, Los Angeles, USA.

Introduction: The Dawn spacecraft, carrying the Framing Cameras, was captured by Ceres' gravity field on 6th March 2015. The FC delivered images [1] during approach, three rotation characterisations, and various completed mapping orbits to resolutions of up to ~140 m/px. In mid-December 2015, Dawn reached the low altitude mapping orbit (LAMO) taking panchromatic FC images with a resolution of ~35 m/px.

We present morphological observations of simple to transitional complex craters in order to determine the simple–to–complex (s–c) transition diameter (see also [2-4]. This parameter depends on the strength of the target material and gravity. If the known s–c transition diameters of various planetary bodies are plotted as a function of their surface gravity, the predicted s–c diameter for Ceres is found along the icy trend at about 10.5 km [3] (Fig. 1) potentially indicating a dominantly icy upper surface composition, consistent with pre-Dawn studies [e.g., 5–7]. However, this is in contrast to the global albedo value of Ceres (c. 0.09) relative to icy satellites (>>0.19). Recent Dawn results indicate an upper crust density of ~1.5 gcm^{-3} [8,9] with an inferred ice–rock ratio of about 40:60 [10]. Both Dawn spectral data taken in Survey Orbit and Earth-based telescopic observations indicate the presence of widespread ammoniated phyllosilicates [11,12], though other Earth-based obsrvations point to a carbonaceous condrite-like surface composition [e.g., 13]. Localised detections of vapour emanation [14], haze cloud development [15], and water absorption bands in Dawn's VIR reflectance spectra [16] indicate heterogeneity in surface composition. A heterogenous composition with respect to ice content is in agreement with thermal modelling [17] and first GRaND results [18]. Determining the s–c transition diameter(s) across Ceres will help understand strength properties of upper surface target material(s).

Method: The presented study was conducted on a global FC image mosaic with a resolution of ~140 m/px. 474 craters in the size range of 3–40 km and distributed across the surface of Ceres were classified. Our analysis will be updated when LAMO imagery becomes available.

Classification scheme: Craters with pristine to mildly degraded morphologies were classified into simple, modified simple, transitional complex, and complex craters. Simple craters are entirely bowl-shaped with steep smooth walls and a circular rim. Modified simple craters are those craters closely resembling simple craters but exhibt a flat floor, which is <0.5D across. The rim crest may be punctuated by small impact craters. Transitional complex craters are characterised by a scalloped rim, a flat floor >0.5D across and the absence of terraces. Complex craters show a flat floor, scalloped rims, and terraces; a central peak may have formed but can be buried by collapsed wall material.

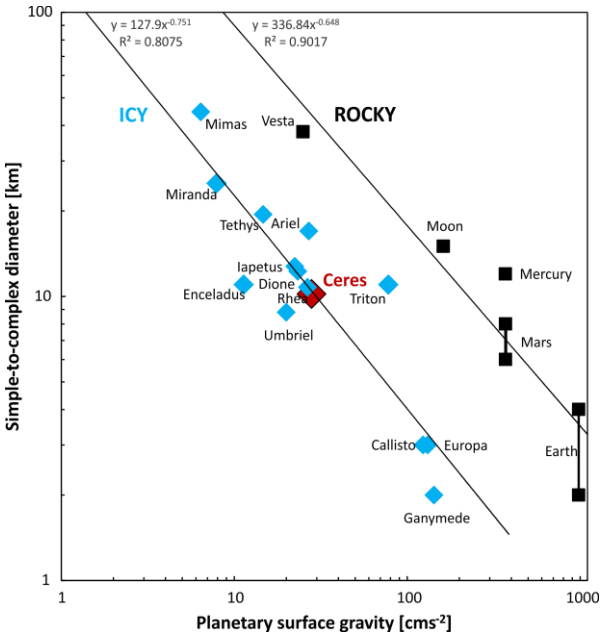

Fig. 1: Simple–to–complex transition diameters for rocky and icy planetary bodies as a function of their surface gravity. Data are from [19–26].

Result: The first global survey shows that simple craters (n=96) occur primarily in the diameter size range from 3–6 km with a maximum diameter of 14.7 km (Fig. 2). The majority of craters (n=257) are classed modified simple craters ranging in diameter from 3.8–19.2 km (average=8.3 km). Transitional complex craters (n=99) are on average 17.8 km in diameter (Fig. 2). We note that only one simple crater in the size range 6–9 km is located in the equatorial region whereas 16 craters occur at higher latitudes (Fig. 3). The largest six simple craters (9–15 km) are found near the north pole (Fig. 3).

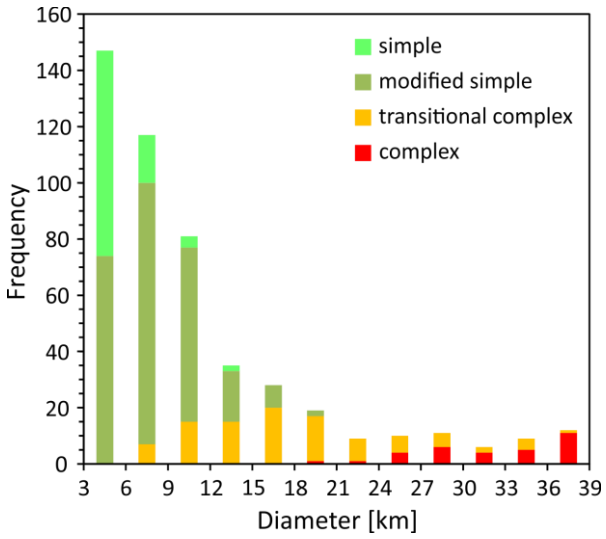

Fig. 2: Frequency plot of classed craters per diameter (bin size is 3 km).

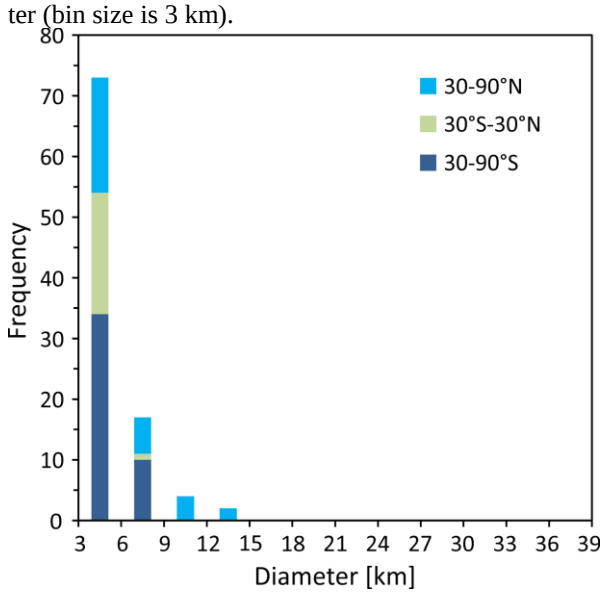

Fig. 3: Frequency plot of simple craters per diameter (bin size is 3 km) differentiated into three regions each spanning 60° latitude.

Discussion: Based on the High Altitude Mapping Orbit imagery (~140 m/px), the s–c transition cannot be clearly assigned and may spread over a larger diameter range. It's minimum estimate, however, is 6 km. As upper bound of the s–c transition the size range 18-21 km is given. First LAMO images already revealed that classified modified simple and transitional complex craters need to be revisted. Floor deposits need to be carefully analysed and interpreted as to whether they simply formed during crater formation, by post-impact wall collapse or external-sourced mass flows. In addition, hummocky/spiral-textured floor material in transitional complex and complex craters may have potentially buried central peaks causing misclassification.

Final LAMO-based crater classification may also confirm a latitudinal dependence of the s–c transition, increasing from the equator towards the poles due to modelled latitudinal temperature differences [17]. Surface gravity changes due to Ceres' oblateness (482×482×446 km) may influence the s–c transition diameter [8]. It will also be investigated whether the s–c transition has any longitudinal variation, correlating with areas of different topographic roughness and relative crater relaxation rates or gravity. Moreover, strength properties of various materials similar to ice will be analysed in order to assess whether rock–ice mixtures, phyllosilicate- or sulphate-dominated regolith may account for the large spread in s–c transition diameters. Another important diagnostic parameter for determining the s–c transition is the diameter–to–depth relationship. A systematic survey of crater depth analysis will be performed and presented at the conference along with the final crater classification and derived conclusions.

Acknowledgement: Support of the Dawn Instrument, Operations, and Science Teams is gratefully acknowledged. This work is supported by grants from NASA through the Dawn project, and from the German and Italian Space Agencies.

References: [1] Sierks H. et al. (2011) *Space Sci Rev*, 163, 263–327. [2] Schenk P. et al. (2015) *EPSC*, EPSC2015-400. [3] Platz T. et al. (2015) *EPSC*, EPSC2015–466. [4] Schenk P. et al. (2016) *LPSC* (this meeting). [5] Thomas P. C. et al. (2005) *Nature*, 437, 224–226. [6] McCord T. B. et al., Space Sci. Rev., 163, 63–76, 2011. [7] Bland M. T. (2013) *Icarus*, 226, 510–521. [8] Ermakov A. et al. (2016) *LPSC* (this meeting). [9] Park R. S. et al. (2016) *LPSC* (this meeting). [10] Bland M. T. et al. (2016) *LPSC* (this meeting). [11] King T. V. V. et al. (1992) *Science*, 255, 1551–1553. [12] De Sanctis M. C. (2015) *Nature*, 528, 241–244. [13] Miliken R. E. and Rivkin A. S. (2009) *NatGeo*, 2, 258–261. [14] Küppers M. et al. (2014) *Nature*, 505, 525–527. [15] Nathues A. et al. (2015) *Nature*, 528, 237–240. [16] Combe J.-P. et al. (2016) *LPSC* (this meeting). [17] Hayne P. O. and Aharonson O. (2015) *JGR*, 120, 1567–1584. [18] Prettyman T. H. et al. (2016) *LPSC* (this meeting). [19] Schenk P. M. (1989) *JGR*, 94, 3813–3832. [20] Schenk P. M. (2002) *Nature*, 417, 419–421. [21] Moore J. M. et al. (2004) *Icarus*, 171, 421–443. [22] White O. L. et al. (2013) *Icarus*, 223, 699–709. [23] Vincent J.-B. et al. (2014) *Planet. Space Sci.*, 103, 57–65. [24] Giese B. et al. (2008) *GRL*, 35, L24204. [25] Strom R. G. et al. (1990) *Science*, 250, 437–439. [26] Barnouin O. S. et al. (2012) *Icarus*, 219, 414-427.